
Reasoning-Enhanced Object-Centric Learning for Videos

Jian Li¹ Pu Ren² Yang Liu³ Hao Sun¹

Abstract

Object-centric learning aims to break down complex visual scenes into more manageable object representations, enhancing the understanding and reasoning abilities of machine learning systems toward the physical world. Recently, slot-based video models have demonstrated remarkable proficiency in segmenting and tracking objects, but they overlook the importance of the effective reasoning module. In the real world, reasoning and predictive abilities play a crucial role in human perception and object tracking; in particular, these abilities are closely related to human intuitive physics. Inspired by this, we designed a novel reasoning module called the Slot-based Time-Space Transformer with Memory buffer (STATM) to enhance the model’s perception ability in complex scenes. The memory buffer primarily serves as storage for slot information from upstream modules, the Slot-based Time-Space Transformer makes predictions through slot-based spatiotemporal attention computations and fusion. Our experiment results on various datasets show that STATM can significantly enhance object-centric learning capabilities of slot-based video models.

1. Introduction

Objects are the fundamental elements that constitute our world, which adhere to the fundamental laws of physics. Humans learn through activities such as observing the world and interacting with it. They utilize the knowledge acquired via these processes for reasoning and prediction. All these aspects are crucial components of human intuitive physics (Lake et al., 2017; Kubricht et al., 2017; Riochet et al., 2018; Smith, 2019). Therefore, object-centric research is pivotal for comprehending human cognitive processes and for developing more intelligent artificial intelligence (AI) systems. By studying the properties, movements, interactions, and be-

haviors of objects, we can uncover the ways and patterns in which humans think and make decisions in the domains of perception, learning, decision-making, and planning. This contributes to the advancement of more sophisticated machine learning algorithms and AI systems, enabling them to better understand and emulate human intuitive physical abilities (Janner et al., 2019; Tang et al., 2023).

Recently, the representative SAVi (Kipf et al., 2021) and SAVi++ (Elsayed et al., 2022) models have demonstrated impressive performance in object perception. SAVi (Slot Attention for Video) employed optical flow as a prediction target and leveraged a small set of abstract hints as conditional inputs in the first frame to acquire object-centric representations of dynamic scenes. SAVi++ (Towards End-to-End Object-Centric Learning from Real-World Videos) enhanced the SAVi by integrating depth prediction and implementing optimal strategies for architectural design and data augmentation. Both SAVi and SAVi++ execute two steps on observed video frames: a prediction step and a correction step. The correction step uses inputs to update the slots. The prediction step uses the slots information of the objects provided by the correction step for prediction. The predictor’s output initializes the correction process in the subsequent time step, ensuring the model’s consistent ability to track objects over time.

The two main steps of such a model operate in a positive feedback loop. The more accurate the predictions, the better the corrections become. Consequently, the more accurate the corrections, the more precise the information provided for the prediction step is, leading to better predictions. Therefore, having a reasonable and efficient predictor is crucial for the entire model. In real-world scenarios, humans also engage in prediction as a crucial aspect of their object perception and tracking, but their prediction behaviors often involve more intricate processes. Humans typically combine the motion state of an object with the interactions of other objects to predict possible future states and positions of the object. The object’s motion state is inferred by humans using their common sense from the object’s past positions over a while. In so doing, humans enhance their ability to recognize and track relevant objects within complex scenes, which is an integral component of human intuitive physics (Sudderth, 2006; Ullman et al., 2017; Mitko & Fischer, 2020). The prediction step in SAVi and SAVi++ is similar

¹Renmin University of China ²Lawrence Berkeley National Lab
³University of Chinese Academy of Sciences. Correspondence to:
Hao Sun <haosun@ruc.edu.cn>.

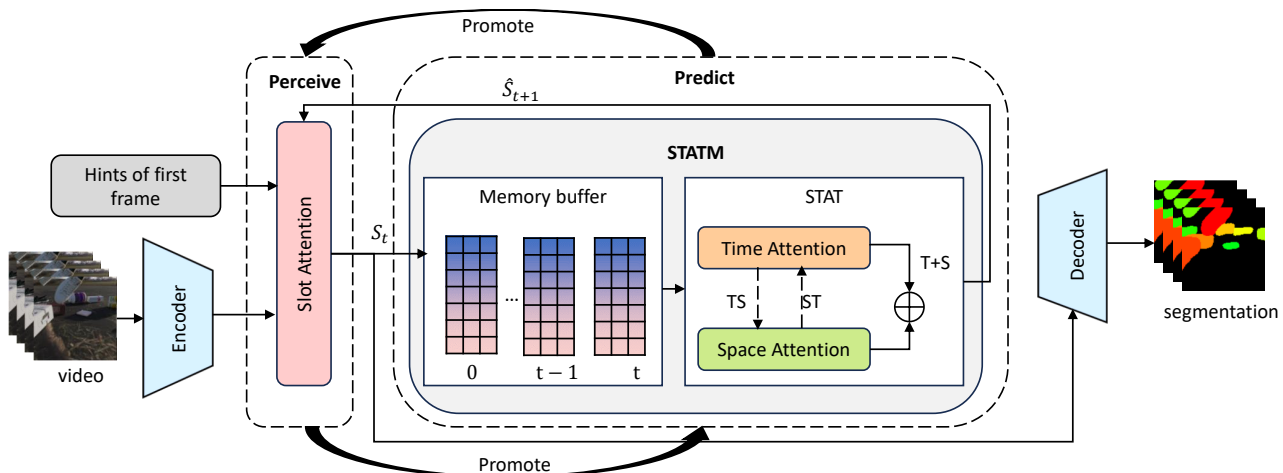


Figure 1. Slot-based Time-Space Transformer with Memory buffer architecture overview.

to human inference, but their predictor module is somewhat simplistic, as it relies solely on single-frame information from the current time step for prediction.

Drawing inspiration from human behavior, we introduce a novel prediction module aimed at enhancing slot-based models for video. This module comprises two key components: 1) Slot-based Memory Buffer: primarily designed to store historical slot information obtained from the upstream modules; and 2) Slot-based Time-Space Transformer Module: designed by applying spatiotemporal attention mechanisms to slots for inferring the temporal motion states of objects and calculating spatial objects interactions, which also integrates time and space attention results. We term the proposed model as *Slot-based Time-Space Transformer with Memory buffer* (STATM). Upon substituting the prediction module of SAVi and SAVi++ into the STATM, we observe distinct impacts of different spatiotemporal fusion methods on SAVi and SAVi++. By employing an appropriate fusion method and memory buffer sizes, we observed a significant enhancement in the object segmentation and tracking capabilities of SAVi and SAVi++ on videos containing complex backgrounds and multiple objects per scene.

2. Related Work

Object-centric Learning. In recent years, object-centric learning has emerged as a significant research direction in computer vision and machine learning. It aims to enable machines to perceive and understand the environment from an object-centered perspective, thereby constructing more intelligent visual systems. There is a rich literature on this research, including SQAIR (Kosiorek et al., 2018), R-SQAIR (Stanić & Schmidhuber, 2019), SCALOR (Jiang et al., 2019), Monet (Burgess et al., 2019), OP3 (Veerapaneni et al., 2020), ViMON (Weis et al., 2020), PSGNet

(Bear et al., 2020), SIMONe (Kabra et al., 2021), and others (Kahneman et al., 1992; Kipf et al., 2019; Zhang et al., 2022; Xie et al., 2022). Slot-based Models represent a prominent approach within object-centric learning. They achieve this by representing each object in a scene as an individual slot, which is used to store object features and attributes (Locatello et al., 2020; Kumar et al., 2020; Zoran et al., 2021; Singh et al., 2021; Yang et al., 2021; Zoran et al., 2021; Ye et al., 2021; Hassanin et al., 2022; Wang et al., 2023; Heravi et al., 2023; Wu et al., 2023).

Prediction and Inference on Physics. The implementation of object-centric physical reasoning is crucial for human intelligence and is also a key objective in artificial intelligence. Interaction Network (Battaglia et al., 2016) as the first general-purpose learnable physics engine, is capable of performing reasoning tasks centered around objects or relationships. Another similar study is the Neural Physics Engine (Chang et al., 2016). On the other hand, Visual Interaction Networks (Watters et al., 2017) can learn physical laws from videos to predict the future states of objects. Additionally, there are many models developed based on this foundation (Henderson & Lampert, 2020; Chen et al., 2021; Dittadi et al., 2021; Jusup et al., 2022; Meng et al., 2022; Piloto et al., 2022; Singh et al., 2022; Driess et al., 2023). In order to achieve a deeper understanding of commonsense intuitive physics within artificial intelligence systems, (Piloto et al., 2022) have built a system capable of learning various physical concepts, albeit requiring access to privileged information such as segmentation. Our research primarily aims to construct an object-centric system for object perception, learning of physics, and reasoning.

Slot-based Attention and spatiotemporal Attention. Our current work is closely related to slot-based attention and spatiotemporal attention. There are a lot of works related to

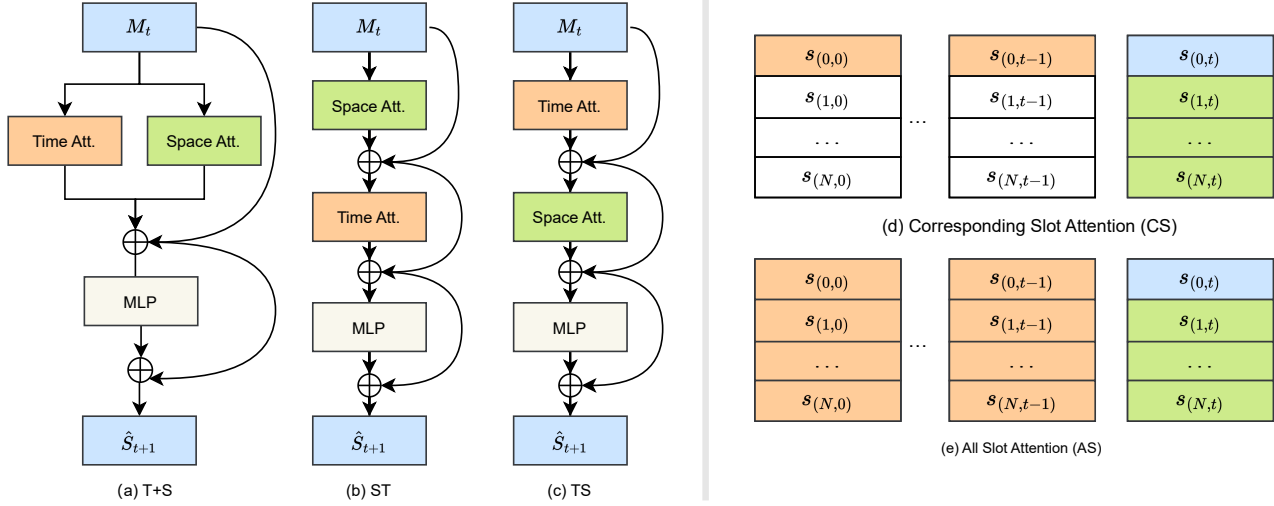


Figure 2. **Left:** Fusion approaches of spatiotemporal attention explored in our study. (a) The sum of computed temporal attention and spatial attention (T+S). (b) Spatial attention computation followed by using the outcome as input for temporal attention (ST). (c) Temporal attention computation followed by using the outcome as input for spatial attention (TS). **Right:** Spatiotemporal attention architectures explored in our study. The green slots represent those employed for spatial attention computation, while the orange slots are indicative of those used for temporal attention computation. (d) Corresponding Slot Attention (CS). (e) All Slot Attention (AS).

slot-based attention (Locatello et al., 2020; Hu et al., 2020; Kumar et al., 2020; Zoran et al., 2021; Singh et al., 2021; Yang et al., 2021; Zoran et al., 2021; Ye et al., 2021; Hasanin et al., 2022; Wang et al., 2023; Heravi et al., 2023; Wu et al., 2023). Spatiotemporal attention mechanisms are particularly effective in handling video data or time-series data, allowing networks to understand and leverage relationships between different time steps or spatial positions (Li et al., 2020; Bertasius et al., 2021; Luo et al., 2021). Currently, they find wide applications in various fields such as video object detection and tracking (Lin et al., 2021; Chen et al., 2022), action recognition (Yang et al., 2022), natural language processing (Xu et al., 2020; Weld et al., 2022), medical image processing (Zhang et al., 2020), among many others (Ding et al., 2020; Yuan et al., 2020; Cheng et al., 2020).

3. Slot-based Time-Space Transformer with Memory Buffer (STATM)

To enhance the slot-based video models, we introduce a new module called the *Slot-based Time-Space Transformer with Memory Buffer* (STATM) as the predictor. STATM is primarily designed to support causal reasoning and prediction for object-centric downstream tasks based on slots. This module consists of two key components: 1) the memory buffer, and 2) the Slot-based Time-Space Transformer (STAT). The memory buffer serves as a repository for storing historical slot information obtained from upstream modules, while

STAT utilizes the information stored in the memory buffer for prediction and causal reasoning.

3.1. Memory Buffer

The memory module is utilized for storing slot information from the upstream modules. We employ a queue-based storage mechanism. The representation of the memory buffer at time t is given by:

$$M_t = \text{Queue}(S_i, \dots, S_t), \quad (1)$$

where $S_t = \{s_{(0,t)}, \dots, s_{(N,t)}\}$ represents the slot information extracted from the corrector module at time t . Here, N signifies the number of slots, which is associated with the number of objects within the scene. The size of M can be fixed or infinite. The new information is appended at the end of the queue.

3.2. Slot-based Time-Space Transformer

The primary role of STAT (Slot-based Time-Space Transformer) lies in leveraging slot data from the memory buffer to facilitate slot-based dynamic temporal reasoning and spatial interaction computations. Furthermore, it integrates the outcomes of temporal reasoning and spatial interactions to achieve a unified understanding. Specifically, for temporal dynamic reasoning, a cross-attention mechanism is employed, which effectively utilizes historical context stored in the memory buffer to enable accurate predictions of future states. Meanwhile, for spatial interaction computations,

we employ a self-attention mechanism that operates on slot representations to compute the relevance between different slots within the S . The results obtained from temporal dynamic reasoning and spatial interaction computation are merged to provide a holistic understanding encompassing both temporal dynamics and spatial interactions. This comprehensive representation enhances the model’s capability for accurate prediction and reasoning in object-centric tasks. We propose three approaches as illustrated in Figure 2 a-c.

We also introduced two computational architectures for spatiotemporal attention as illustrated in Figure 2 d-e. (1) *Corresponding Slot Attention (CS)*: For slot $s_{(i,t)}$, temporal attention is computed by using it and corresponding slots in $\{s_{(i,0)}, \dots, s_{(i,t-1)}\}$, while spatial attention computation is performed using it and all slots within $\{s_{(0,t)}, \dots, s_{(N,t)}\}$. (2) *All Slot Attention (AS)*: For slot $s_{(i,t)}$, temporal attention is computed by using it and all slots in $\{s_{(0,0)}, \dots, s_{(N,t-1)}\}$. The spatial attention computation remains the same as in approach CS.

In the CS architecture, $s_{(i,t)}$ undergoes temporal attention computation exclusively with its corresponding slots. This design offers several notable advantages. Firstly, it enables a more robust association between objects and slots in terms of temporal sequences, preserving the slot’s invariance with respect to the object. Additionally, this approach significantly reduces computational costs when compared to the AS structure. This efficiency makes the CS architecture an appealing choice for achieving effective temporal binding while optimizing computational resources.

In the AS architecture, the temporal attention involves calculating the attention between $s_{(i,t)}$ and all previous slots. The AS structure is designed to achieve improved slot-based prediction and reasoning in complex, unguided scenarios. In previous time steps, objects were not effectively bound to specific slots, requiring each slot to search through memory to link relevant object information. The AS architecture assumes that objects were not segmented in previous frames or that effective hints for segmentation were absent.

In summary, if the upstream task effectively segments objects into slots, the CS architecture is preferred. Otherwise, the AS architecture can be considered.

For slot-based models with hints in the first frame, the AS enhancement might not be significantly effective and could increase computational load. We adopt the CS attention architecture with the T+S spatiotemporal fusion approach for our proposed STATM predictor. The memory buffer stores the slot information from the corrector for time steps. We then explain the calculation of spatiotemporal attention:

$$M_t = \text{Queue}(S_0, \dots, S_t). \quad (2)$$

For a STAT encoding block, query/key/value vectors are

computed for each slot:

$$k_{(i,t)}^a = LN_k^a(s_{(i,t)}) \in R^{D_h}, \quad (3a)$$

$$q_{(i,t)}^a = LN_q^a(s_{(i,t)}) \in R^{D_h}, \quad (3b)$$

$$v_{(i,t)}^a = LN_v^a(s_{(i,t)}) \in R^{D_h}, \quad (3c)$$

where k , q , and v represent learned linear projections. $s_{(i,t)}$ denotes the vector of the i -th slot at time t . The latent dimensionality for each attention head is set to $D_h = D/A$.

The computation of spatiotemporal attention is also slot-based, and weights are calculated using dot-product. For the slot $s_{(i,t)}$, the spatiotemporal attention weights are computed as follows:

$$a_{(i,t)}^{(a)time} = \text{Softmax} \left(\left(\frac{q_{(i,t)}^{(a)}}{\sqrt{D_h}} \right)^T \cdot \left[k_{(i,0)}^{(a)} \left\{ k_{(i',t')}^{(a)} \right\}_{t'=1, \dots, T} \right] \right),$$

$$a_{(i,t)}^{(a)space} = \text{Softmax} \left(\left(\frac{q_{(i,t)}^{(a)}}{\sqrt{D_h}} \right)^T \cdot \left[k_{(0,t)}^{(a)} \left\{ k_{(i',t)}^{(a)} \right\}_{i'=1, \dots, N} \right] \right). \quad (4)$$

For each slot at time t , we calculate the weighted sum of value vectors using spatiotemporal attention coefficients from each attention head. The individual temporal or spatial attention systems in the CS structure refer to Equation (5).

$$z_{(i,t)}^{(a)time} = \sum_{t'=0}^T a_{(i,t),(t')}^{(a)time} v_{(i,t')}^{(a)}, \quad (5a)$$

$$z_{(i,t)}^{(a)space} = \sum_{i'=0}^N a_{(i,t),(i')}^{(a)space} v_{(i',t)}^{(a)}. \quad (5b)$$

The combined spatiotemporal vectors are individually linearly transformed, summed, and input into an MLP, where layer normalization (LN) is applied after each residual structure, *v.i.z.*,

$$s'_{(i,t)}{}^{time} = W_o^{time} \begin{bmatrix} z_{(i,t)}^{(1)time} \\ \vdots \\ z_{(i,t)}^{(A)time} \end{bmatrix} + s_{(i,t)}, \quad (6a)$$

$$s'_{(i,t)}{}^{space} = W_o^{space} \begin{bmatrix} z_{(i,t)}^{(1)space} \\ \vdots \\ z_{(i,t)}^{(A)space} \end{bmatrix} + s_{(i,t)}, \quad (6b)$$

$$s'_{(i,t)} = \text{LN} \left(s'_{(i,t)}{}^{time} + s'_{(i,t)}{}^{space} \right), \quad (7a)$$

$$\hat{s}_{(i,t+1)} = \text{LN} \left(\text{MLP} \left(s'_{(i,t)} \right) + s'_{(i,t)} \right). \quad (7b)$$

In this section, we focus on the computation process of the CS architecture using the T+S fusion approach for the

STAT encoding block. In summary, temporal attention is calculated by jointly incorporating historical information from the memory buffer and spatial attention’s slot $s_{(i,t)}$. Across all structural approaches, computations are based on slots, and the equation formulations remain consistent.

4. Experiments

The central aims of our experiments include: 1) To validate the efficacy of our model, incorporating STATM as a substitute for the transformer encoding block predictor within the SAVi and SAVi++ frameworks. 2) To investigate the effects of varying memory buffer sizes during both the training and inference stages on the performance of the model. 3) To assess the impact of different spatiotemporal methods integrated within STATM on the model’s effectiveness.

Metrics. We selected the Adjusted Rand Index (ARI) (Rand, 1971; Hubert & Arabie, 1985) and the mean Intersection over Union (mIoU) as evaluation metrics. ARI quantifies the alignment between predicted and ground-truth segmentation masks. For scene decomposition assessment, we commonly employ FG-ARI, which is a permutation-invariant clustering similarity metric. It allows us to compare inferred segmentation masks to ground-truth masks while excluding background pixels. mIoU is a widely used segmentation metric that calculates the mean Intersection over Union values for different classes or objects in a segmentation task. It measures the overlap between the predicted segmentation masks and the ground-truth masks, indicating the quality of object segmentation. In the context of video analysis, mIoU is adapted to evaluate the consistency and accuracy of object segmentation and tracking across frames. It provides insights into how well the model captures the spatial relationships between objects in consecutive frames.

Datasets. To evaluate the performance of our model, we utilized the synthetic Multi-Object Video (MOVi) datasets (Research, 2020; Greff et al., 2022). These datasets are divided into five distinct categories: A, B, C, D, and E. MOVi-A and B depict relatively straightforward scenes, each containing a maximum of 10 objects. MOVi-C, D, and E present more intricate scenarios with complex natural backgrounds. MOVi-C, generated using a stationary camera, presents scenes with up to 10 objects. Transitioning to MOVi-D, the dataset extends the object count to accommodate a maximum of 23 objects. Lastly, MOVi-E introduces an additional layer of complexity by incorporating random linear camera movements. Each video sequence is sampled at a rate of 12 frames per second, resulting in a total of 24 frames per second.

Training Setup. We conducted our experiments in JAX (Bradbury et al., 2018) using the Flax (Heek et al., 2020) neural network library. In all experiments except the abla-

tion study in Section 4.2, we used the STAT encoding block in combination with the CS attention architecture, featuring the T+S spatiotemporal fusion approach. For training the STATM-SAVi and SAVi models, we utilized videos comprising of 6 frames at a resolution of 64×64 pixels. The training process is conducted over 100k iterations. Similarly, the STATM-SAVi++ and SAVi++ models were trained on continuous videos consisting of 6 frames at a higher resolution of 128×128 pixels, with training duration encompassing 100k or 500k iterations. The buffer size was unconstrained during training, and the maximum length of effective information was limited to 6 due to the utilization of a 6-frame training sequence. Bounding boxes were used as the conditioning for all models. For more training setup, please refer to Appendix B.

4.1. Improvement with STATM

Results. Quantitative results can be seen in Table 1, and qualitative results in Figure 3. In all cases, our models were trained on 6 consecutive frames, but we present results for full (24-frame) sequences at test time. From Table 1, it is evident that our models perform significantly better than the original model. Comparing SAVi and STATM-SAVi, SAVi performs reasonably well on simple datasets but poorly on complex datasets. As the complexity of the datasets increases, the advantage of STATM-SAVi over SAVi becomes more pronounced. In comparison between SAVi++ and STATM-SAVi++, the enhanced model shows a notable improvement, and except for the MOVi-E (due to insufficient training), it can generally match or surpass the optimal results of SAVi++. Further, when considering the best results of STATM-SAVi++* against the official results SAVi++, our model’s performance is markedly superior to the original model, indicating that the model’s benefits do not diminish with increased training. The limitations of depth information and overfitting mentioned in the SAVi++ (Elsayed et al., 2022) do not appear in STATM-SAVi++. The qualitative results from Figure 3 also demonstrate the superior performance of our models (e.g., the notable difference between SAVi and STATM-SAVi in the first frame of MOVi-A). In addition, we provide more qualitative results and visualizations of attention maps for Slot Attention. Please refer to Appendix D for more results.

From Figure 4, it is evident that both SAVi and SAVi++ face challenges in recognizing newly appearing objects and objects that reappear after being occluded. When a new object emerges, the original algorithm often misidentifies it as background or an already occupied slot is taken over by the new object. With the incorporation of STATM, although the model may not immediately segment the new object, as the historical information accumulates in the memory buffer, the STAT module can gradually provide the corrector with hints required for the object segmentation (e.g., position or

Table 1. Segmentation results on the MOVi dataset. The first four rows depict the evaluation results for models trained for 100k steps with a batch size of 32. SAVi++* represents results from SAVi++ paper (Elsayed et al., 2022). STATM-SAVi++* denotes the evaluation results for STATM-SAVi++ model trained for 500k steps with a batch size of 64 (Mean \pm standard error over 3 seeds).

Model	mIoU \uparrow (%)					FG-ARI \uparrow (%)				
	A	B	C	D	E	A	B	C	D	E
SAVi-S	62.8	41.6	22.0	6.8	4.0	91.1	70.2	50.4	18.4	10.8
STATM-SAVi-S	67.5	42.8	34.0	17.0	9.0	91.1	70.1	57.7	40.9	36.9
SAVi++	82.8	52.5	47.8	43.6	26.1	96.7	78.5	76.3	81.5	81.7
STATM-SAVi++	83.5	52.5	49.5	50.1	27.9	96.9	78.9	77.7	85.8	85.0
SAVi++*	76.1 \pm 0.9	25.8 \pm 11.3	45.2 \pm 0.1	48.3 \pm 0.5	47.1 \pm 1.3	98.2 \pm 0.2	48.3 \pm 15.7	81.9 \pm 0.2	86.0 \pm 0.3	84.1 \pm 0.9
STATM-SAVi++*	85.6\pm0.6	60.4\pm1.2	52.4\pm0.2	57.0\pm0.4	55.4\pm0.9	98.3\pm0.2	84.9\pm2.5	82.2\pm0.2	89.1\pm0.2	88.6\pm0.5

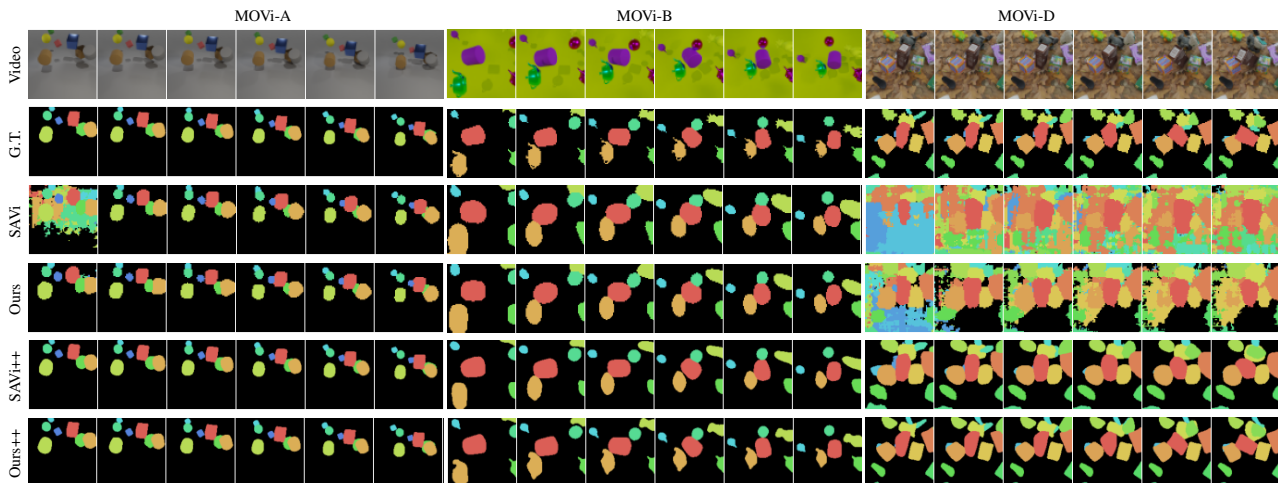


Figure 3. Qualitative results of our model compared to SAVi and SAVi++ on the MOVi dataset. Compared with SAVi and SAVi++, our model is slightly better than the SAVi/SAVi++ mode on the relatively simple datasets. As the complexity of the datasets increases, the advantage of our model becomes more pronounced.

shape), eventually, the model can successfully segment the object. When an object disappears (possibly temporarily occluded), SAVi++ immediately releases the slot associated with the object, potentially causing difficulty in binding the object to the original slot or even failing to recognize it upon reappearance. For STATM-SAVi++, due to the presence of the memory buffer and temporal attention in STATM, when the occluded object reappears, it can easily be assigned to its historical slot. Only when the object has been absent for an extended period will the slot be released.

In addition, we also tried to use the STATM module to improve the unsupervised scene segmentation model STEVE. The results can be found in the Appendix D.

Generalization. We utilized test sets featuring scenes exclusively comprising previously unseen objects and backgrounds to assess the improved model’s generalization during testing. The results are depicted in Figure 5 (a). Notably, our model exhibits strong generalization capabilities to unfamiliar objects and backgrounds. For additional details,

please refer to Appendix D.

Discussion. Certainly, the STATM module, acting as a predictor, significantly enhances the model performance of SAVi and SAVi++. Compared to the original models, the improved model can achieve good performance with fewer training steps and a smaller batch size. STATM-SAVi++ also addresses the overfitting issue of SAVi++ on simple datasets (especially noticeable in MOVi-B). The enhanced models also exhibit good generalization.

4.2. Ablation Study

In this section, we aim to evaluate the influence of different components of STATM, using STATM-SAVi as a baseline. Given the indispensability of the memory module, we focus on two key aspects: 1) The effect of memory buffer size on the model during both training and inference phases; and 2) The influence of different spatiotemporal attention competition and fusion methods on the model.

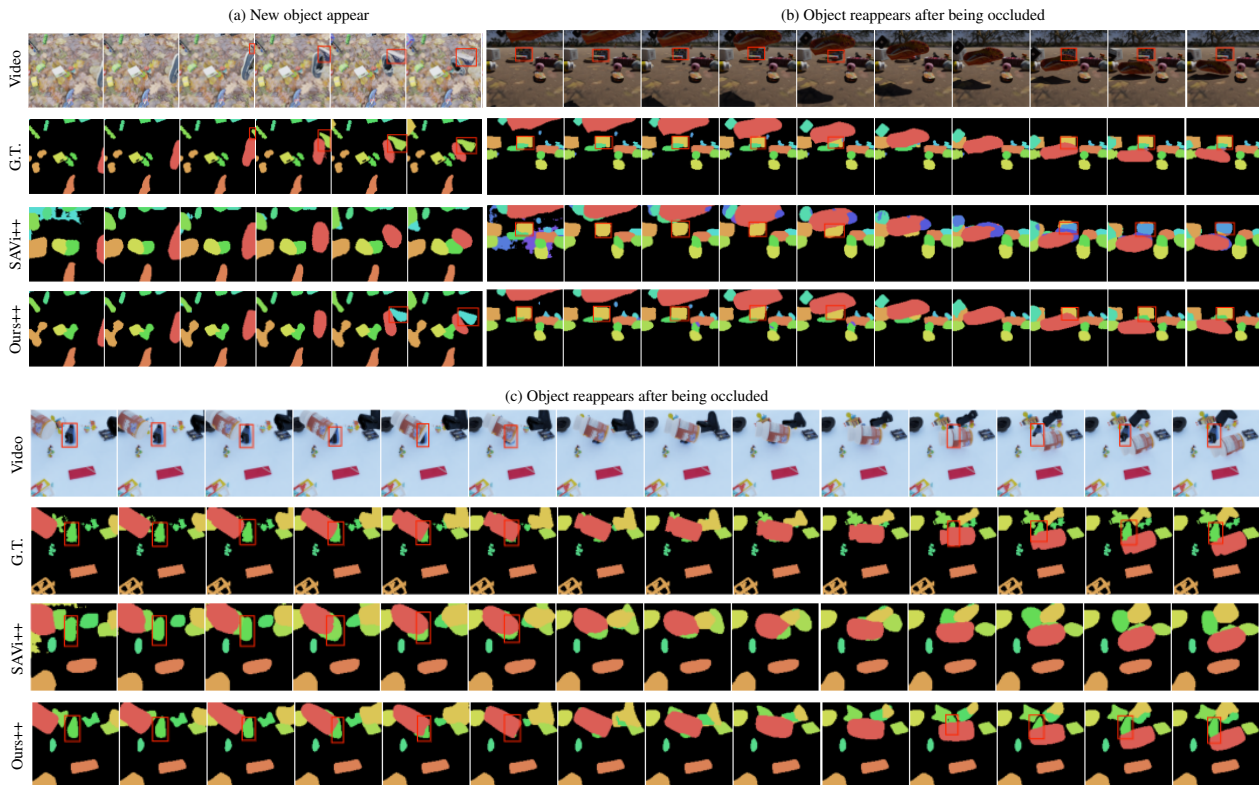


Figure 4. Qualitative results of our model compared to SAVi++. (a) When a new object appears, the original algorithm cannot recognize it, but our model can correctly identifies it after 1-2 frames. (b) and (c) When an object reappears after being obscured, the original algorithm either assigns it to a different slot (color change) or fails to recognize it. In contrast, our model can correctly identify it.

Ablation Experiment of Memory Module. We have designed two sets of experiments to evaluate the impact of the memory buffer: 1) In the first set, we allowed an unlimited memory buffer length during training, but restricted it to a fixed length during testing, ensuring it didn’t exceed the training buffer’s length. To facilitate evaluation, we have not only assessed the model trained with 6 frames but also extended the training frames to 12, with the 12-frame results available in Appendix E. 2) In the second set, we fixed the buffer length during training, not exceeding the maximum buffer length, and removed any buffer length restrictions during testing. We show results for full (24-frame) sequences during test time in Figure 5 (b) and (c).

Longer-duration video processing presents a challenge to the prediction and inference abilities of the model. It requires that the model extrapolate the learned physical laws of object motion to previously invisible segments. Therefore, the buffer’s role during the testing becomes crucial for inference, especially for object tracking and segmentation beyond the training frame number (see Figure 5 (b)). The prediction module requires additional information to summarize the physical laws of object motion, enabling it to make accurate predictions.

Limiting the buffer length during the training phase reduces the segmentation and tracking capabilities of the model, but the decline is not overly serious. The model’s tracking and segmentation capabilities over a duration equal to the training frames are less affected by memory (see Figure 5 (c)). For more detailed analysis, please refer to Appendix E.

In summary, increasing the memory buffer size during both training and testing phases benefits the improvement of the model’s perceptual capabilities across all datasets. However, for particularly complex datasets like MOVi-E, the excessive increase in the number of training frames may lead to a decline in the model’s segmentation capabilities. In such cases, it might be worth considering improvements to modules like the encoder or corrector to enhance feature extraction capabilities.

Ablation Experiments of Spatiotemporal Fusion and Computation. We conducted ablation experiments of the spatiotemporal fusion method via the CS structure on the MOVi-A dataset. For the ablation experiments related to the spatiotemporal computation structure, we chose the T+S fusion method. Since the AS structure was primarily designed for complex datasets, the computation method ablation experiments were conducted on the MOVi-E dataset. All

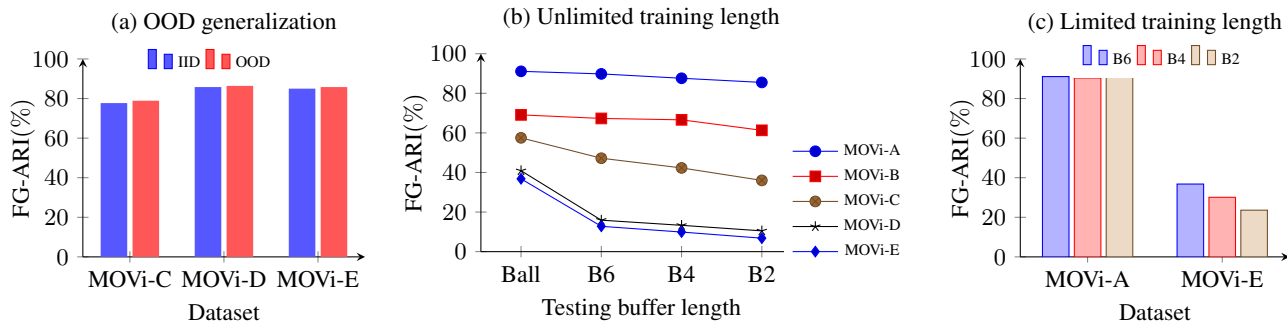


Figure 5. **Left:** (a) Video decomposition results on out-of-distribution evaluation splits with new objects and new backgrounds. **Right:** Segmentation results with different memory buffers on the MOVi dataset. (b) During training, all available information is utilized with an unlimited buffer length. The x -axis represents the model results during testing with buffer sizes ranging from unlimited to limited (6, 4, and 2 frames). (c) Training the model using sub-sequences of 6 frames. The different bars represent the model results during training with buffer sizes of 6, 4, and 2 frames.

Table 2. Result of spatiotemporal fusion method.

Model	mIoU \uparrow (%)		FG-ARI \uparrow (%)	
	A	E	A	E
STATM (CS, ST)	58.4	-	90.9	-
STATM (CS, TS)	61.2	-	89.7	-
STATM (CS, T+S)	67.5	8.5	91.1	36.8
STATM (AS, T+S)	-	3.8	-	12.2

models were trained using the first 6 frames of the video. The experimental results can be found in Table 2.

On the MOVi-E dataset, the segmentation capability of the AS structure is not as robust as that of the CS structure, but its FG-ARI still outperforms the baseline. This suggests the following. 1) Compared to the transform encoding block, it produces more precise predictions for the STATM encoding block with the AS structure as the predictor, enhancing the object segmentation and tracking abilities of slot-based models like SAVi in complex video scenes. 2) As mentioned earlier, the AS structure is designed to handle scenes where objects are not effectively segmented into corresponding slots. Appendix E indicates that with the assistance of initial frame cues, SAVi exhibits decent scene decomposition in the early frames of test videos from the MOVi-E dataset. However, as time progresses, the lack of dynamic temporal interactions among corresponding slots and the impact of complex backgrounds lead to declining segmentation and tracking performance. Currently, models without prompts have limited relevance to our objectives. Hence, we choose not to conduct extensive experiments to verify the capabilities of the STATM with the AS structure.

4.3. Limitations

We used STATM as a prediction module to enhance the perceptual capabilities of slot-based models. However, we didn’t assess our model using real-world datasets. The

foundation of our model’s construction is based on the principle that “prediction and correction mutually reinforce each other”. However, our evaluation of the rationality and effectiveness of STATM is based on the experimental results from the correction step, and we haven’t directly tested its physical learning and reasoning abilities. We hope to get a model that performs well in both perception and prediction, which remains an important focus of our future research. In addition, our model may experience a delay (1-2 frames) in recognizing new objects, and the non-immediate release of slots after an object disappears may lead to an insufficient number of slots (more slots needed than the maximum number of objects in the scene).

5. Conclusion

In the real world, all objects follow the laws of physics. Intuitive physics serves as the bridge and connection through which humans comprehend the world. Our research aims to construct biologically plausible deep learning models to explore whether deep learning models can learn physical concepts like humans, and use these learned physical laws to make inferences and predictions about the future motion of objects.

We have designed a more reasonable prediction module called STATM, which clearly improved slot-based models in the context of scene understanding and prediction. We demonstrated that reasoning and prediction abilities influence the model’s scene object segmentation and tracking. The more accurate the reasoning and prediction abilities, the stronger the segmentation and tracking of objects. Through a series of experiments, we investigated the influence of memory and spatiotemporal reasoning on the model’s perceptual abilities. Although there still remain many challenges on this topic, the results in this paper illustrate that well-designed deep learning models can mimic human perception. In the future, we will continue to explore more cognitive

theories as a basis and continue to work hard to obtain a model that performs well in both perception and prediction.

References

- Battaglia, P., Pascanu, R., Lai, M., Jimenez Rezende, D., et al. Interaction networks for learning about objects, relations and physics. *Advances in neural information processing systems*, 29, 2016.
- Bear, D., Fan, C., Mrowca, D., Li, Y., Alter, S., Nayebi, A., Schwartz, J., Fei-Fei, L. F., Wu, J., Tenenbaum, J., et al. Learning physical graph representations from visual scenes. *Advances in Neural Information Processing Systems*, 33:6027–6039, 2020.
- Bertasius, G., Wang, H., and Torresani, L. Is space-time attention all you need for video understanding? In *ICML*, volume 2, pp. 4, 2021.
- Bradbury, J., Frostig, R., Hawkins, P., Johnson, M. J., Leary, C., Maclaurin, D., Necula, G., Paszke, A., VanderPlas, J., Wanderman-Milne, S., et al. Jax: composable transformations of python+ numpy programs. 2018.
- Burgess, C. P., Matthey, L., Watters, N., Kabra, R., Higgins, I., Botvinick, M., and Lerchner, A. Monet: Unsupervised scene decomposition and representation. *arXiv preprint arXiv:1901.11390*, 2019.
- Chang, M. B., Ullman, T., Torralba, A., and Tenenbaum, J. B. A compositional object-based approach to learning physical dynamics. *arXiv preprint arXiv:1612.00341*, 2016.
- Chen, B., Li, T., and Ding, W. Detecting deepfake videos based on spatiotemporal attention and convolutional lstm. *Information Sciences*, 601:58–70, 2022.
- Chen, C., Deng, F., and Ahn, S. Roots: Object-centric representation and rendering of 3d scenes. *The Journal of Machine Learning Research*, 22(1):11770–11805, 2021.
- Cheng, D., Xiang, S., Shang, C., Zhang, Y., Yang, F., and Zhang, L. Spatio-temporal attention-based neural network for credit card fraud detection. In *Proceedings of the AAAI conference on artificial intelligence*, volume 34, pp. 362–369, 2020.
- Ding, Y., Zhu, Y., Feng, J., Zhang, P., and Cheng, Z. Interpretable spatio-temporal attention lstm model for flood forecasting. *Neurocomputing*, 403:348–359, 2020.
- Dittadi, A., Papa, S., De Vita, M., Schölkopf, B., Winther, O., and Locatello, F. Generalization and robustness implications in object-centric learning. *arXiv preprint arXiv:2107.00637*, 2021.
- Driess, D., Huang, Z., Li, Y., Tedrake, R., and Toussaint, M. Learning multi-object dynamics with compositional neural radiance fields. In *Conference on Robot Learning*, pp. 1755–1768. PMLR, 2023.
- Elsayed, G., Mahendran, A., van Steenkiste, S., Greff, K., Mozer, M. C., and Kipf, T. Savi++: Towards end-to-end object-centric learning from real-world videos. *Advances in Neural Information Processing Systems*, 35:28940–28954, 2022.
- Greff, K., Belletti, F., Beyer, L., Doersch, C., Du, Y., Duckworth, D., Fleet, D. J., Gnanaprasadam, D., Golemo, F., Herrmann, C., et al. Kubric: A scalable dataset generator. In *Proceedings of the IEEE/CVF Conference on Computer Vision and Pattern Recognition*, pp. 3749–3761, 2022.
- Hassanin, M., Anwar, S., Radwan, I., Khan, F. S., and Mian, A. Visual attention methods in deep learning: An in-depth survey. *arXiv preprint arXiv:2204.07756*, 2022.
- Heek, J., Levskaya, A., Oliver, A., Ritter, M., Rondepierre, B., Steiner, A., and van Zee, M. Flax: A neural network library and ecosystem for jax, 2020. *URL <http://github.com/google/flax>*, 1, 2020.
- Henderson, P. and Lampert, C. H. Unsupervised object-centric video generation and decomposition in 3d. *Advances in Neural Information Processing Systems*, 33: 3106–3117, 2020.
- Heravi, N., Wahid, A., Lynch, C., Florence, P., Armstrong, T., Tompson, J., Sermanet, P., Bohg, J., and Dwibedi, D. Visuomotor control in multi-object scenes using object-aware representations. In *2023 IEEE International Conference on Robotics and Automation (ICRA)*, pp. 9515–9522. IEEE, 2023.
- Hu, J., Yang, Y., Chen, C., He, L., and Yu, Z. Sas: Dialogue state tracking via slot attention and slot information sharing. In *Proceedings of the 58th annual meeting of the association for computational linguistics*, pp. 6366–6375, 2020.
- Hubert, L. and Arabie, P. Comparing partitions. *Journal of classification*, 2:193–218, 1985.
- Im, D., Ahn, S., Memisevic, R., and Bengio, Y. Denoising criterion for variational auto-encoding framework. In *Proceedings of the AAAI conference on artificial intelligence*, volume 31, 2017.
- Janner, M., Levine, S., Freeman, W. T., Tenenbaum, J. B., Finn, C., and Wu, J. Reasoning about physical interactions with object-oriented prediction and planning. In *International Conference on Learning Representations*, 2019.

- Jiang, J., Janghorbani, S., De Melo, G., and Ahn, S. Scalor: Generative world models with scalable object representations. *arXiv preprint arXiv:1910.02384*, 2019.
- Jusup, M., Holme, P., Kanazawa, K., Takayasu, M., Romić, I., Wang, Z., Geček, S., Lipić, T., Podobnik, B., Wang, L., et al. Social physics. *Physics Reports*, 948:1–148, 2022.
- Kabra, R., Zoran, D., Erdogan, G., Matthey, L., Creswell, A., Botvinick, M., Lerchner, A., and Burgess, C. Simone: View-invariant, temporally-abstracted object representations via unsupervised video decomposition. *Advances in Neural Information Processing Systems*, 34:20146–20159, 2021.
- Kahneman, D., Treisman, A., and Gibbs, B. J. The reviewing of object files: Object-specific integration of information. *Cognitive psychology*, 24(2):175–219, 1992.
- Kingma, D. P. and Ba, J. Adam: A method for stochastic optimization. *arXiv preprint arXiv:1412.6980*, 2014.
- Kipf, T., Van der Pol, E., and Welling, M. Contrastive learning of structured world models. *arXiv preprint arXiv:1911.12247*, 2019.
- Kipf, T., Elsayed, G. F., Mahendran, A., Stone, A., Sabour, S., Heigold, G., Jonschkowski, R., Dosovitskiy, A., and Greff, K. Conditional object-centric learning from video. In *International Conference on Learning Representations*, 2021.
- Kosiorrek, A., Kim, H., Teh, Y. W., and Posner, I. Sequential attend, infer, repeat: Generative modelling of moving objects. *Advances in Neural Information Processing Systems*, 31, 2018.
- Kubricht, J. R., Holyoak, K. J., and Lu, H. Intuitive physics: Current research and controversies. *Trends in cognitive sciences*, 21(10):749–759, 2017.
- Kumar, A., Ku, P., Goyal, A., Metallinou, A., and Hakkani-Tur, D. Ma-dst: Multi-attention-based scalable dialog state tracking. In *Proceedings of the AAAI conference on artificial intelligence*, volume 34, pp. 8107–8114, 2020.
- Lake, B. M., Ullman, T. D., Tenenbaum, J. B., and Gershman, S. J. Building machines that learn and think like people. *Behavioral and brain sciences*, 40:e253, 2017.
- Li, J., Liu, X., Zhang, W., Zhang, M., Song, J., and Sebe, N. Spatio-temporal attention networks for action recognition and detection. *IEEE Transactions on Multimedia*, 22(11): 2990–3001, 2020.
- Lin, L., Li, W., Bi, H., and Qin, L. Vehicle trajectory prediction using lstms with spatial-temporal attention mechanisms. *IEEE Intelligent Transportation Systems Magazine*, 14(2):197–208, 2021.
- Locatello, F., Weissenborn, D., Unterthiner, T., Mahendran, A., Heigold, G., Uszkoreit, J., Dosovitskiy, A., and Kipf, T. Object-centric learning with slot attention. *Advances in Neural Information Processing Systems*, 33:11525–11538, 2020.
- Loshchilov, I. and Hutter, F. Sgdr: Stochastic gradient descent with warm restarts. *arXiv preprint arXiv:1608.03983*, 2016.
- Luo, Y., Liu, Q., and Liu, Z. Stan: Spatio-temporal attention network for next location recommendation. In *Proceedings of the web conference 2021*, pp. 2177–2185, 2021.
- Meng, C., Seo, S., Cao, D., Griesemer, S., and Liu, Y. When physics meets machine learning: A survey of physics-informed machine learning. *arXiv preprint arXiv:2203.16797*, 2022.
- Mitko, A. and Fischer, J. When it all falls down: the relationship between intuitive physics and spatial cognition. *Cognitive research: principles and implications*, 5:1–13, 2020.
- Paszke, A., Gross, S., Massa, F., Lerer, A., Bradbury, J., Chanan, G., Killeen, T., Lin, Z., Gimelshein, N., Antiga, L., et al. Pytorch: An imperative style, high-performance deep learning library. *Advances in neural information processing systems*, 32, 2019.
- Piloto, L. S., Weinstein, A., Battaglia, P., and Botvinick, M. Intuitive physics learning in a deep-learning model inspired by developmental psychology. *Nature human behaviour*, 6(9):1257–1267, 2022.
- Rand, W. M. Objective criteria for the evaluation of clustering methods. *Journal of the American Statistical association*, 66(336):846–850, 1971.
- Research, G. Google scanned objects, 2020. URL <https://app.ignitionrobotics.org/GoogleResearch/fuel/collections/Google%20Scanned%20Objects>.
- Riochet, R., Castro, M. Y., Bernard, M., Lerer, A., Fergus, R., Izard, V., and Dupoux, E. Intphys: A framework and benchmark for visual intuitive physics reasoning. *arXiv preprint arXiv:1803.07616*, 2018.
- Singh, G., Deng, F., and Ahn, S. Illiterate dall-e learns to compose. *arXiv preprint arXiv:2110.11405*, 2021.
- Singh, G., Wu, Y.-F., and Ahn, S. Simple unsupervised object-centric learning for complex and naturalistic videos. *Advances in Neural Information Processing Systems*, 35:18181–18196, 2022.

- Smith, B. C. *The promise of artificial intelligence: reckoning and judgment*. Mit Press, 2019.
- Stanić, A. and Schmidhuber, J. R-sqair: Relational sequential attend, infer, repeat. *arXiv preprint arXiv:1910.05231*, 2019.
- Sudderth, E. B. *Graphical models for visual object recognition and tracking*. PhD thesis, Massachusetts Institute of Technology, 2006.
- Tang, Q., Zhu, X., Lei, Z., and Zhang, Z. Intrinsic physical concepts discovery with object-centric predictive models. In *Proceedings of the IEEE/CVF Conference on Computer Vision and Pattern Recognition*, pp. 23252–23261, 2023.
- Ullman, T. D., Spelke, E., Battaglia, P., and Tenenbaum, J. B. Mind games: Game engines as an architecture for intuitive physics. *Trends in cognitive sciences*, 21(9): 649–665, 2017.
- Vaswani, A., Shazeer, N., Parmar, N., Uszkoreit, J., Jones, L., Gomez, A. N., Kaiser, Ł., and Polosukhin, I. Attention is all you need. *Advances in neural information processing systems*, 30, 2017.
- Veerapaneni, R., Co-Reyes, J. D., Chang, M., Janner, M., Finn, C., Wu, J., Tenenbaum, J., and Levine, S. Entity abstraction in visual model-based reinforcement learning. In *Conference on Robot Learning*, pp. 1439–1456. PMLR, 2020.
- Wang, Y., Liu, L., and Dauwels, J. Slot-vae: Object-centric scene generation with slot attention. *arXiv preprint arXiv:2306.06997*, 2023.
- Watters, N., Zoran, D., Weber, T., Battaglia, P., Pascanu, R., and Tacchetti, A. Visual interaction networks: Learning a physics simulator from video. *Advances in neural information processing systems*, 30, 2017.
- Watters, N., Matthey, L., Burgess, C. P., and Lerchner, A. Spatial broadcast decoder: A simple architecture for learning disentangled representations in vaes. *arXiv preprint arXiv:1901.07017*, 2019.
- Weis, M. A., Chitta, K., Sharma, Y., Brendel, W., Bethge, M., Geiger, A., and Ecker, A. S. Unmasking the inductive biases of unsupervised object representations for video sequences. *arXiv preprint arXiv:2006.07034*, 2, 2020.
- Weld, H., Huang, X., Long, S., Poon, J., and Han, S. C. A survey of joint intent detection and slot filling models in natural language understanding. *ACM Computing Surveys*, 55(8):1–38, 2022.
- Wu, Z., Dvornik, N., Greff, K., Kipf, T., and Garg, A. Slotformer: Unsupervised visual dynamics simulation with object-centric models. In *The Eleventh International Conference on Learning Representations*, 2023. URL <https://openreview.net/forum?id=TFbwV6I0VLg>.
- Xie, J., Xie, W., and Zisserman, A. Segmenting moving objects via an object-centric layered representation. *Advances in Neural Information Processing Systems*, 35: 28023–28036, 2022.
- Xu, W., Haider, B., and Mansour, S. End-to-end slot alignment and recognition for cross-lingual nlu. *arXiv preprint arXiv:2004.14353*, 2020.
- Yang, C., Lamdouar, H., Lu, E., Zisserman, A., and Xie, W. Self-supervised video object segmentation by motion grouping. In *Proceedings of the IEEE/CVF International Conference on Computer Vision*, pp. 7177–7188, 2021.
- Yang, D., Zhang, H., Yurtsever, E., Redmill, K. A., and Özgüner, Ü. Predicting pedestrian crossing intention with feature fusion and spatio-temporal attention. *IEEE Transactions on Intelligent Vehicles*, 7(2):221–230, 2022.
- Ye, F., Manotumruksa, J., Zhang, Q., Li, S., and Yilmaz, E. Slot self-attentive dialogue state tracking. In *Proceedings of the Web Conference 2021*, pp. 1598–1608, 2021.
- Yuan, X., Li, L., Shardt, Y. A., Wang, Y., and Yang, C. Deep learning with spatiotemporal attention-based lstm for industrial soft sensor model development. *IEEE Transactions on Industrial Electronics*, 68(5):4404–4414, 2020.
- Zhang, C., Gupta, A., and Zisserman, A. Is an object-centric video representation beneficial for transfer? In *Proceedings of the Asian Conference on Computer Vision*, pp. 1976–1994, 2022.
- Zhang, J., Liu, A., Gao, M., Chen, X., Zhang, X., and Chen, X. Ecg-based multi-class arrhythmia detection using spatio-temporal attention-based convolutional recurrent neural network. *Artificial Intelligence in Medicine*, 106: 101856, 2020.
- Zoran, D., Kabra, R., Lerchner, A., and Rezende, D. J. Parts: Unsupervised segmentation with slots, attention and independence maximization. In *Proceedings of the IEEE/CVF International Conference on Computer Vision*, pp. 10439–10447, 2021.

A. Baselines

To validate the effectiveness of STATM, we chose three baselines which are state-of-the-art in object-centric video scene decomposition for improvement and comparison. All three models include a similar module: Slot Attention (Locatello et al., 2020) followed by a predictor (a transformer encoder block (Vaswani et al., 2017)).

SAVi. The SAVi model (Kipf et al., 2021) consists of five main components: encoder, decoder, slot initialization, corrector, and predictor. The encoder utilizes a convolutional neural network as a backbone to extract features from input video frames. The slot initialization is either a simple MLP (in the case of bounding boxes or center of mass coordinates) or a convolutional neural network (in the case of segmentation masks), responsible for initializing slots based on the conditioning information (bounding boxes, center of mass coordinates, or segmentation masks) in the first frame. The corrector employs Slot Attention (Locatello et al., 2020) to update slot information based on visual features from the encoder. The predictor, a transformer encoder block (Vaswani et al., 2017), utilizes self-attention among the slots for prediction. The output of the predictor initializes the corrector at the next time step, ensuring consistent object tracking over time. Finally, the decoder uses a Spatial Broadcast Decoder (Watters et al., 2019) to generate RGB predictions of optical flow (or reconstructed frames) and an alpha mask.

For the SAVi model, we chose the official implementation of SAVi with a small CNN as backbone, which is trained and evaluated on downscaled 64*64 frames. We initialized the slots in the first frame using bounding boxes as hints (slot initialization is a simple MLP). Since one of the main contributions of the SAVi model is using optical flow as a self-supervised objectives, we selected optical flow as the target for training the model. During training, we adjusted the batch size to 32, while keeping other settings and parameters the same as SAVi-small.

SAVi++. SAVi++ (Elsayed et al., 2022) has a structure similar to SAVi with a ResNet34 backbone and consists of five main components: encoder, decoder, slot initialization, corrector, and predictor. Unlike SAVi, SAVi++ introduces depth as self-supervised objectives. It also incorporates data augmentation and utilizes a transformer encoder after ResNet34.

During the training of SAVi++, we adjusted the batch size to 32, the number of training steps to 100k, while keeping other parameters consistent with described in SAVi++. For SAVi+*, the hyperparameters are same as the official implementation.

STEVE. STEVE (Singh et al., 2022) is an unsupervised object-centric scene decomposition model. This baseline employs discrete VAE (Im et al., 2017) for encoding and reconstructing input frames x_t and generating discrete targets (hard sampling) for the transformer decoder. It uses a similar structure combined with the encoder, corrector, and predictor in SAVi, called the recurrent slot encoder, to decompose input video frames x_t into slots. The slot-transformer decoder uses the slots obtained from the recurrent slot encoder to learn to predict the sampling targets from discrete VAE by minimizing the cross-entropy loss. We make no modifications to the official implementation of STEVE.

B. Additional Training Setup

Experiments of STATM-SAVi and STATM-SAVi++. Referring to Section 4.1, we train our models (STATM-SAVi and STATM-SAVi++) for 100k steps with a batch size of 32 using Adam (Kingma & Ba, 2014). Same as SAVi++ (Elsayed et al., 2022), we linearly increase the learning rate for 5000 steps to 0.0002 (starting from 0) and then decay the learning rate with a Cosine schedule (Loshchilov & Hutter, 2016). We split each video into sub-sequences of 6 frames to train the model (In the ablation experiment studying the impact of training stage buffer size on the model, sub-sequences are set to 4/6/12, referring to Section 4.2). In the initialization of slots for the first frame, bounding boxes are utilized as contextual cues. For MOVi-A, B, and C datasets, the number of slots is set to 11. In the case of datasets MOVi-D and E, the number of slots is set to 24. We use 1 iteration per frame for the Slot Attention (Locatello et al., 2020) module. All other parameters and settings for each model remain consistent with their respective baselines. We implement models in JAX using the Flax neural network library, unless stated otherwise. We train all models on 8*4090 GPUs with 24GB memory each (We also trained the model on A100 with 80GB memory or 3090 with 24GB memory. However, for the sake of convenience in time calculations, we standardized the timing to the specifications of the 4090). STATM-SAVi-small takes approximately 8hs for the MOVi-A, B and C datasets, and 9hs for the MOVi-D and E datasets. STATM-SAVi++ takes approximately 9hs for the MOVi-A, B and C datasets, and 17hs for the MOVi-D and E datasets.

Experiments of STATM-SAVi+*. Further, we modify the training steps to 500k and change the batch size to 64 to train the STATM-SAVi++ model. Additionally, for the Slot Attention on the MOVi-E dataset, we adjust the number of iterations to 2 per frame. All other parameters and settings remain consistent with the SAVi++ paper (Elsayed et al., 2022). We train

the model on the MOVi-A, B and C datasets using 8*4090 GPUs with 24GB memory each, which takes about 4 days. For the MOVi-D and E datasets, we used 8*H800 GPUs with 80GB memory each to train the model, and the training process takes about 8 days.

Experiments of STATM-STEVE. Due to the necessity of memory in STATM, we modify the training sub-sequence length to 3/6/24 (corresponding to batch sizes of 24/12/8). All other parameters and settings remain consistent with the STEVE paper (Singh et al., 2022). The model is trained on 2*A100 with 80GB memory each, and 500 epochs require approximately 6 days. We implement STATM-STEVE in PyTorch (Paszke et al., 2019).

C. Additional Parameter

Using the STATM structure as a predictor does lead to a slight increase in the parameter count of the SAVi and SAVi++ models. However, under the same training settings, our model achieves superior metrics. This suggests that the moderate increase in the parameter count doesn’t significantly increase the training complexity of our model.

STATM-SAVi-Small indeed has a parameter increase of approximately 66K compared to SAVi-Small, which is notably smaller than the parameter increase seen in SAVi-Large compared to SAVi-Small (around 21378K parameters). Moreover, our STATM-SAVi-Small model, trained for 100k steps with a batch size of 32, performs similarly to the official SAVi-Large model, trained for 500k steps with a batch size of 64. This further highlights the reasonableness and superiority of our designed prediction module.

Table 3. Comparison of the parameter number for different models.

Model	Parameter Number	Model	Parameter Number
SAVi-Small	895,268	STATM-SAVi-Small	961,572
SAVi-Medium	1,140,740	STATM-SAVi-Medium	1,207,044
SAVi-Large	22,273,412	STATM-SAVi-Large	22,339,716
SAVi++	23,132,165	STATM-SAVi++	23,264,389

D. Additional Experimental Results

Additional Segmentation Results. In order to better assess our model, we conducted an evaluation using the first 6 frames of the videos. Detailed results can be found in Table 4. Referring to Table 1 in the main text, we can observe the following trends: on simple datasets, the decline in our model’s object segmentation and tracking capabilities over extended time sequences is comparable to that of the baseline model. However, on complex datasets like MOVi-C, D, and E, the decrease in our model’s performance is significantly less than that of the baseline model. This indicates that the STATM is more suitable for handling object segmentation and tracking tasks in longer-time sequences and complex environments. This finding further validates the effectiveness of our STATM model.

Table 4. Segmentation results on the first 6 frames of the MOVi dataset.

Model	mIoU \uparrow (%)					FG-ARI \uparrow (%)				
	A	B	C	D	E	A	B	C	D	E
SAVi-S	66.9	49.3	29.7	13.9	8.3	92.3	80.1	69.2	45.5	32.2
STATM-SAVi-S	71.0	51.6	43.5	21.9	12.5	92.6	81.7	73.0	50.2	54.7
SAVi++	85.2	59.5	55.3	49.8	30.7	97.2	86.3	83.9	87.1	88.2
STATM-SAVi++	85.8	59.8	56.8	56.7	31.1	97.2	86.6	83.9	89.2	88.6

Additional Comparison of STEVE Results. STEVE (Singh et al., 2022) is a supervised baseline which is state-of-the-art in object-centric video scene decomposition. It includes a structure similar to SAVi, consisting of an encoder, corrector, and predictor, referred to as the recurrent slot encoder. Therefore, we modified the STEVE model using the STATM module and conducted a brief evaluation of the modified model on the MOVi-D and E datasets. (Note that the STATM structure in STATM-STEVE differs slightly from that in STATM-SAVi. For details, please refer to Appendix F).

From the FG-ARI scores in Table 5, it can be observed that the STATM module improves the segmentation performance of the STEVE on MOVi-D and E datasets. However, STEVE mainly focuses on scene segmentation and does not report mIoU, we don't compare mIoU. During the experiments, we found that the STATM-STEVE model is sensitive to the MSE loss in discrete VAE (Im et al., 2017), and the addition of STATM slightly increases the difficulty of fitting of the model, which becomes more pronounced with an increase in the buffer size of STATM module. Therefore, for a better improvement and testing of the impact of STATM on STEVE, a two-stage training approach can be attempted, where a discrete VAE is first trained, followed by the training of STATM and other modules.

Table 5. Segmentation results on the MOVi-D and E datasets.

Model	MOVi-D	MOVi-E
STEVE	47.67	52.15
STATM-STEVE	51.73	55.78

Additional Qualitative Results. We show more qualitative results on longer time series in Figure 6 to Figure 10.

Visualization of the Attention Map. To analyze slots and better illustrate the relationship between objects and slots, we visualized the attention map of the Slot Attention (corrector) in Figure 11 to Figure 15.

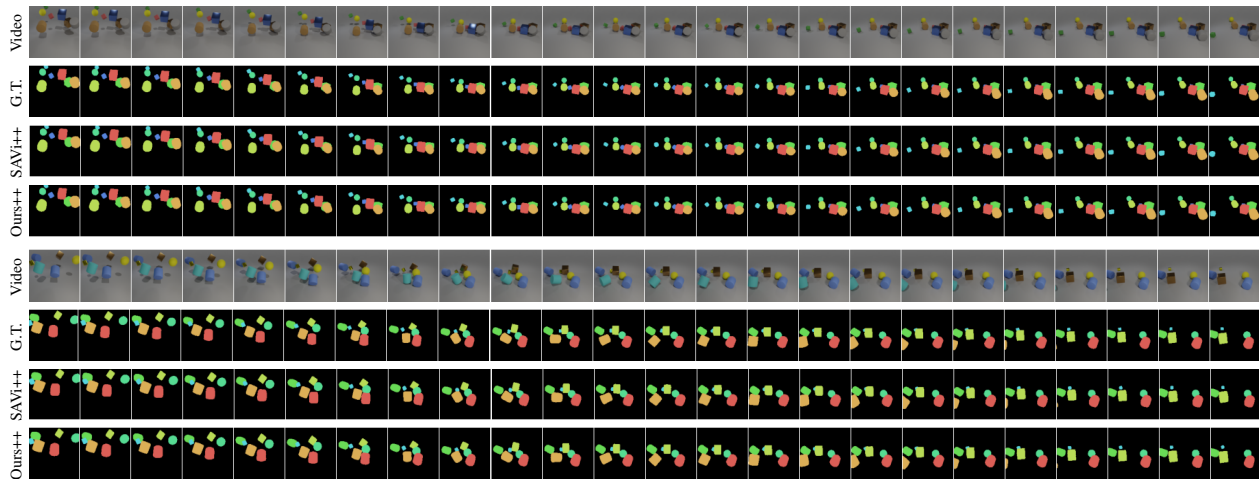


Figure 6. Qualitative results of our model compared to SAVi++ on the MOVi-A dataset.

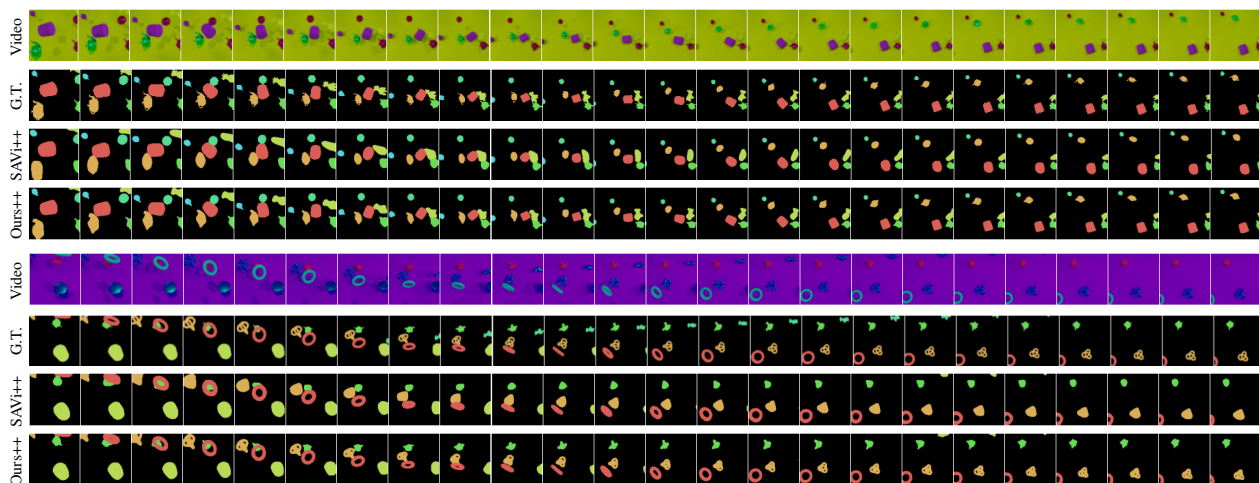


Figure 7. Qualitative results of our model compared to SAVi++ on the MOVi-B dataset.

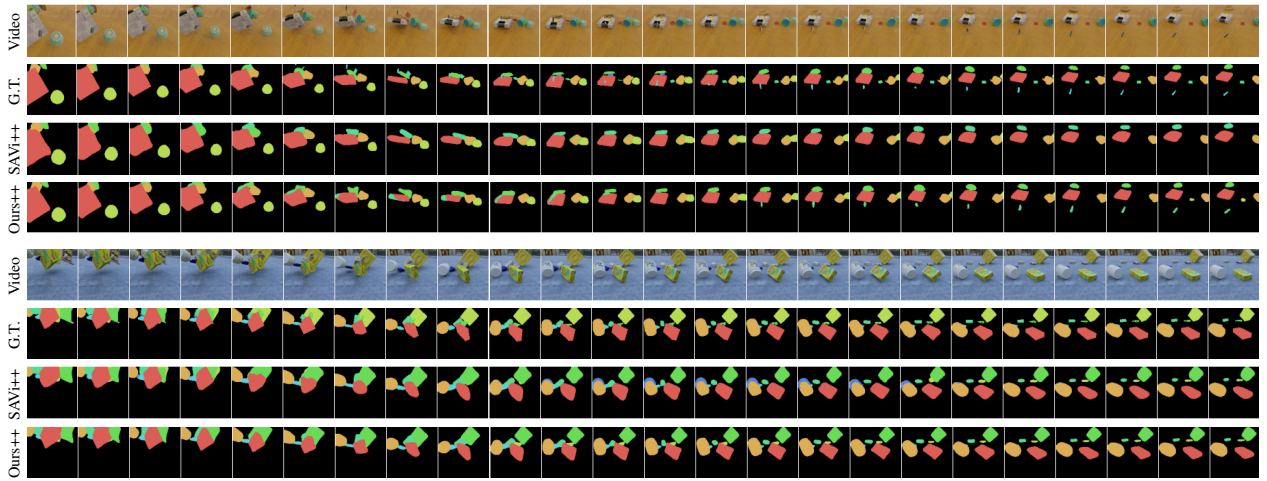


Figure 8. Qualitative results of our model compared to SAVi++ on the MOVi-C dataset.

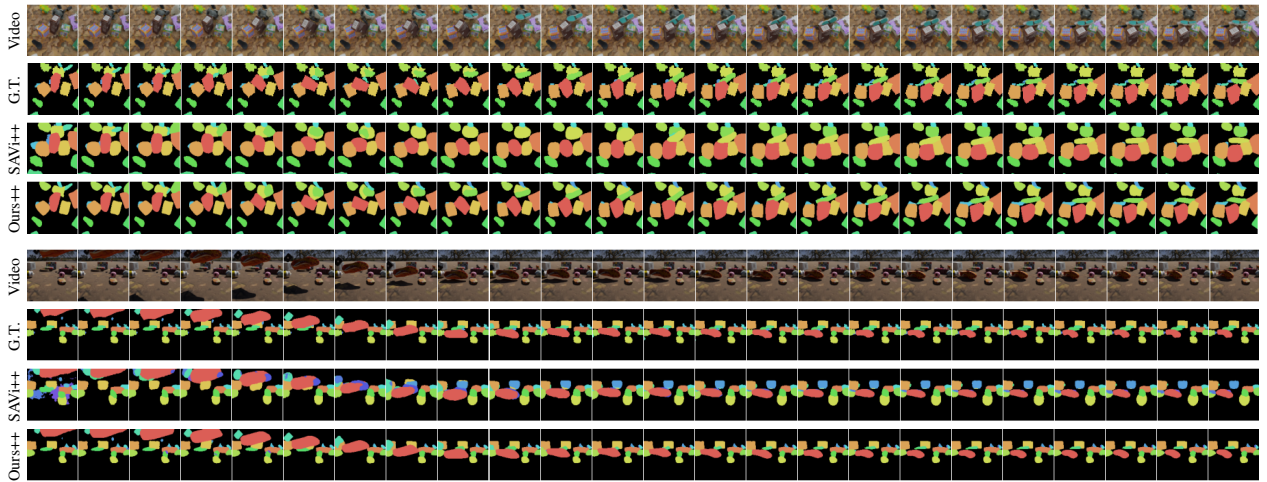


Figure 9. Qualitative results of our model compared to SAVi++ on the MOVi-D dataset.



Figure 10. Qualitative results of our model compared to SAVi++ on the MOVi-E dataset.



Figure 11. Attention map visualization on the MOVi-A dataset.



Figure 12. Attention map visualization on the MOVi-B dataset.

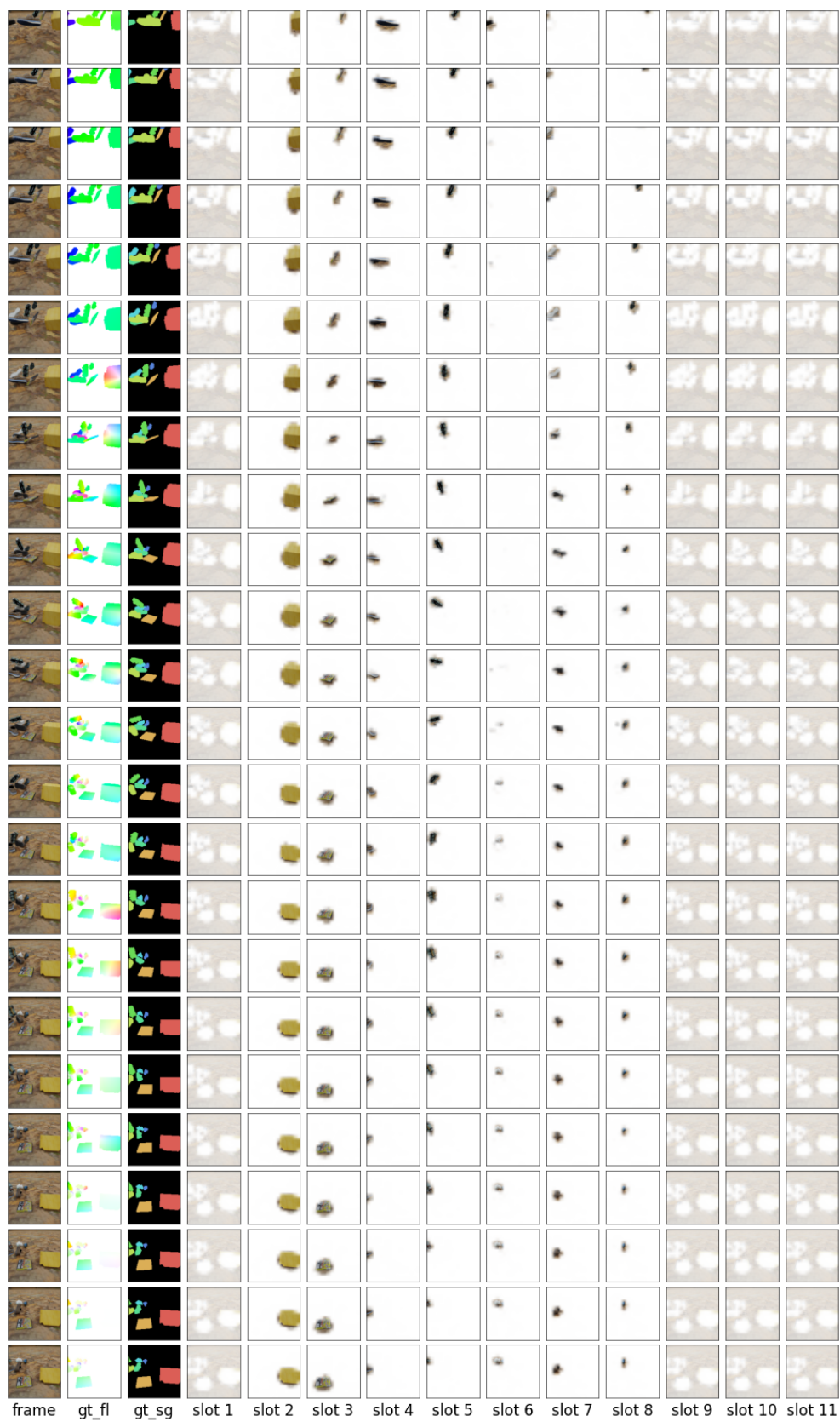


Figure 13. Attention map visualization on the MOVi-C dataset.

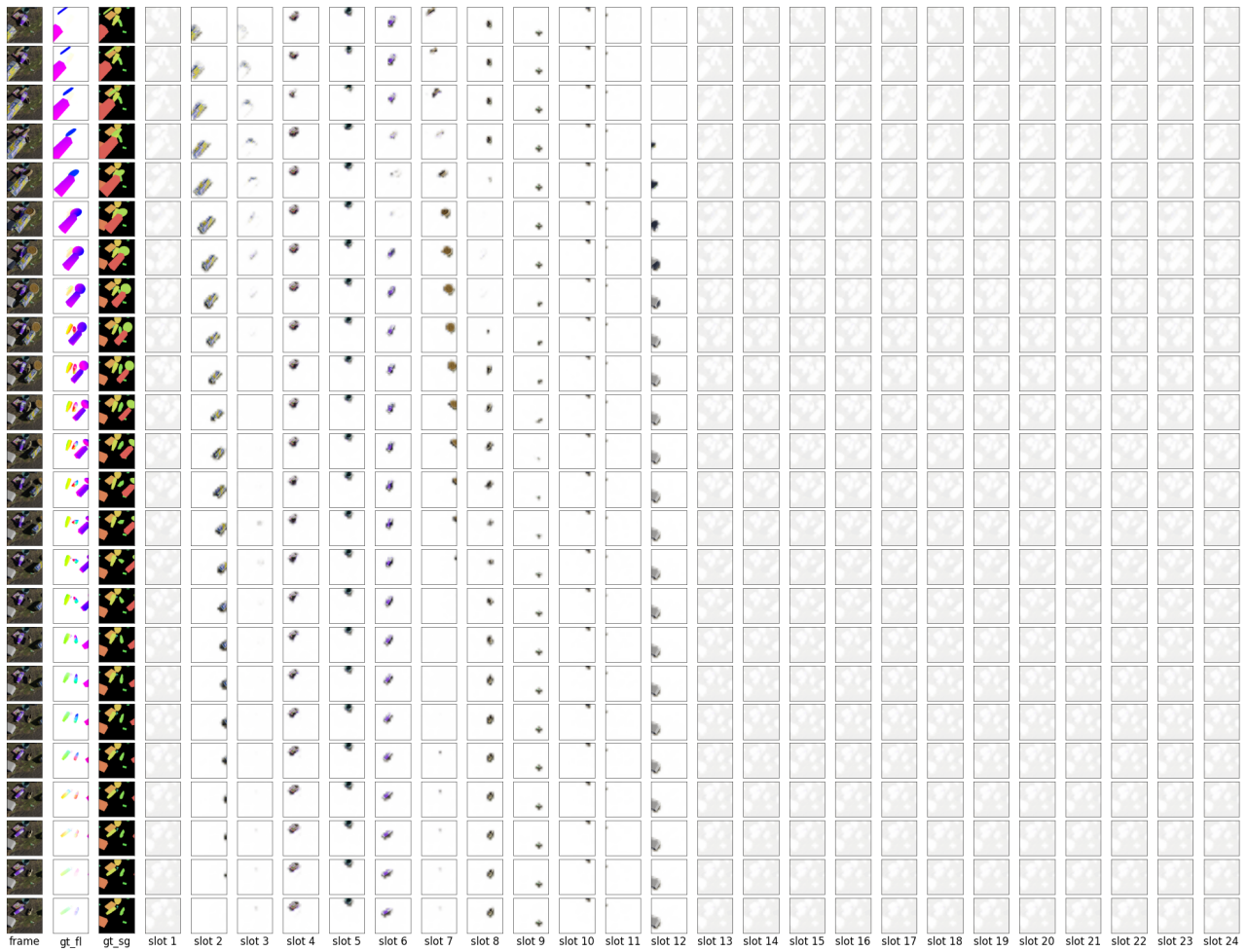


Figure 14. Attention map visualization on the MOVi-D dataset.

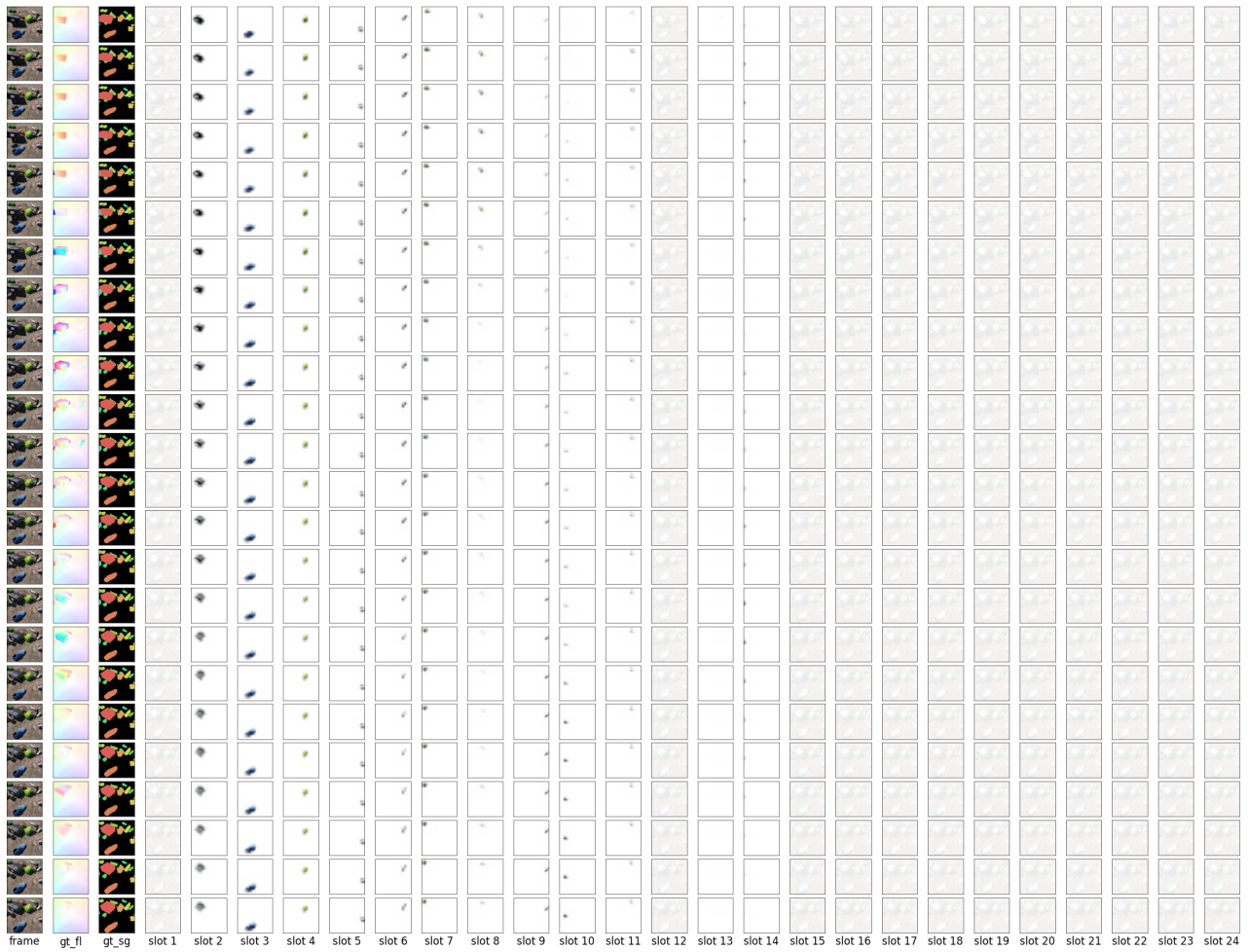


Figure 15. Attention map visualization on the MOVIE dataset.

Additional Generalization Results. We selected the models trained with a batch size of 32 and 100k training steps to assess its generalization. The test set utilized the default test split of MOVi-C, D and E dataset, featuring scenes exclusively consist of held-out objects and background images to evaluate generalization. The results are presented in Table 6.

Table 6. OOD generalization results of STATM-SAVi and STATM-SAVi++ on the MOVi dataset.

Model	mIoU \uparrow (%)			FG-ARI \uparrow (%)		
	C	D	E	C	D	E
STATM-SAVi-S (IID)	34.0	17.0	9.0	57.7	40.9	36.9
STATM-SAVi-S (OOD)	33.2	17.0	8.2	59.7	43.4	35.9
STATM-SAVi++ (IID)	49.5	50.1	27.9	77.7	85.8	85.0
STATM-SAVi++ (OOD)	48.7	50.3	27.4	78.9	86.4	85.8

Additional Metrics. All models were trained in a conditional setting, initializing slots using ground-truth bounding box information in the first frame. Consequently, the results for STATM-SAVi++* in Table 1 are measured from the second frame onward, aligning with the evaluation method in SAVi++ (Elsayed et al., 2022). All other evaluation results include data from the first frame.

E. Additional Ablation Experiment of Memory Module

Training with unlimited buffer length and testing with limited buffer length. To better assess the impact of the buffer on the model, we trained the model using video sub-sequences of 12 frames, as shown in Table 7 and 8. We observed that: 1) On relatively simple datasets like MOVi-A, B, C, and D dataset, increasing the amount of training data with additional information would enhance the model’s segmentation capabilities. 2) Training with a buffer size of 12 results in a decrease in mIoU. SAVi++ augments the number of samples by utilizing sub-sequences of 6 frames. However, in this case, sub-sequences of 12 frames are employed, leading to a reduction in both the number of samples and hints (each sample contains hints in the first frame, so the reduction in the number of samples also reduces the hints). The decrease in both samples and hints may impact the model’s ability to separate foreground and background, consequently causing a decline in mIoU. 3) On the MOVi-E dataset, increasing the number of training frames resulted in a decrease in the model’s tracking and segmentation capabilities. This could be attributed to the limitations in the ability of the upstream modules to effectively extract image features. The findings from the SAVi and SAVi++, which used more powerful encoders and data augmentation to improve segmentation performance on MOVi-E, support this observation. Therefore, exploring the design of a more robust encoder and refining the corrector and guidance modules may yield unexpected improvements. We plan to further investigate this direction in future research.

Training with limited buffer length and testing with limited buffer length. We intentionally limited the buffer size during both the training and testing phases, and the model evaluation results are presented in Table 9. Remarkably, we found that the model trained with a smaller buffer (equivalent to restricted vision) experienced less impact from the buffer during the testing phase. For instance, consider a model trained with a buffer size of 2. When tested with a reduced buffer size on the MOVi-E dataset, the model experienced an approximately 8% decrease in FG-ARI (from 23.6% to 15.5%). On the other hand, when testing with a reduced buffer size on the MOVi-E dataset, a model trained with a buffer size of 6 exhibited a FG-ARI decrease of about 30% (from 36.8% to 6.8%). This has intriguing implications for the fusion of deep learning and

Table 7. Evaluation on all video frames of the model trained using 12 frames (B represents the size of the buffer during the testing phase).

Model	mIoU \uparrow (%)					FG-ARI \uparrow (%)				
	A	B	C	D	E	A	B	C	D	E
STATM (Ball)	66.9	39.3	26.1	13.8	4.3	92.3	72.9	62.5	59.6	17.9
STATM (B12)	66.2	39.3	25.9	13.2	3.9	91.3	73.0	60.8	55.6	10.4
STATM (B6)	64.3	39.3	25.4	12.3	3.6	89.3	72.7	57.4	50.6	5.6
STATM (B4)	62.8	39.1	24.8	11.8	3.4	88.4	72.5	55.1	47.7	4.4
STATM (B2)	59.1	38.2	23.9	11.2	3.1	85.5	70.6	51.1	44.0	3.5

Table 8. Evaluation on the first 6 video frames of the models trained by 6 frames and 12 frames (T represents the number of frames used for training model, B represents the size of the buffer during the testing phase).

Model	mIoU \uparrow (%)					FG-ARI \uparrow (%)				
	A	B	C	D	E	A	B	C	D	E
STATM (T6, Ball)	71.0	51.6	43.5	21.9	12.5	92.6	81.7	73.0	50.2	54.7
STATM (T6, B6)	71.0	51.6	43.5	21.9	12.5	92.6	81.7	73.0	50.2	54.7
STATM (T6, B4)	71.0	51.3	42.7	19.7	12.0	92.6	81.7	72.5	46.8	51.0
STATM (T6, B2)	70.8	49.2	38.7	14.9	10.2	91.8	80.6	69.1	34.6	37.3
STATM (T12, Ball)	60.2	42.7	28.1	15.4	7.6	92.7	82.9	73.6	55.5	33.5
STATM (T12, B12)	60.2	42.7	28.1	15.4	7.6	92.7	82.9	73.6	55.5	33.5
STATM (T12, B6)	60.2	42.7	28.1	15.4	7.6	92.7	82.9	73.6	55.5	33.5
STATM (T12, B4)	59.7	42.8	28.0	15.4	7.3	92.1	82.9	73.3	54.5	29.3
STATM (T12, B2)	58.3	42.5	27.7	14.9	6.4	89.6	82.5	71.6	50.2	19.4

Table 9. Evaluation result of the model trained limited buffer length (T represents the size of the buffer during the training phase, B represents the size of the buffer during the testing phase).

Model	mIoU \uparrow (%)				FG-ARI \uparrow (%)			
	First 6 frames		All frames		First 6 frames		All frames	
	A	E	A	E	A	E	A	E
STATM (T2, Ball)	71.6	9.9	66.9	6.2	92.6	41.2	90.7	23.6
STATM (T2, B6)	71.6	9.9	69.0	5.7	92.6	41.2	91.5	22.7
STATM (T2, B4)	71.7	9.9	69.3	5.4	92.6	41.5	91.2	20.0
STATM (T2, B2)	71.9	9.5	69.5	4.8	92.6	41.3	91.2	15.5
STATM (T4, Ball)	73.6	9.8	68.0	6.8	92.5	41.7	90.4	30.1
STATM (T4, B6)	73.6	9.8	69.5	4.7	92.5	41.7	90.3	15.1
STATM (T4, B4)	73.7	9.7	69.6	4.3	92.4	41.3	90.1	11.8
STATM (T4, B2)	74.0	9.0	69.3	3.9	92.1	38.4	89.2	9.1
STATM (T6, Ball)	71.0	12.5	67.5	8.5	92.6	54.7	91.1	36.8
STATM (T6, B6)	71.0	12.5	66.1	5.4	92.6	54.7	89.8	12.8
STATM (T6, B4)	71.0	12.0	64.2	4.9	92.6	51.0	87.6	9.9
STATM (T6, B2)	70.8	10.2	61.6	4.2	91.8	37.3	85.5	6.8

cognitive science. However, it’s important to note that real human learning and cognitive processes are likely more complex and influenced by various factors. This study provides a theoretical framework, but further theoretical substantiation and experimental validation are still needed.

F. STATM Structure in Different Model

Due to the differences between the SAVi/SAVi++ and STEVE models, there are certain distinctions in the enhanced models' STATM module as well. The following is a simplified algorithm for the STATM module in different models:

Table 10. Simplified algorithm for the STATM module in different models.

STATM in STATM-SAVi /SAVi++	STATM in STATM-STEVE
Input: S_t, M_t	Input: S_t, M_t
	$S_t = \text{LayerNorm}(S_t)$
	$M_t = \text{LayerNorm}(M_t)$
$X_t = \text{Spatiotemporal Attention}(S_t, M_t, M_t)$	$X_t = \text{Spatiotemporal Attention}(S_t, M_t, M_t)$
$X_t = \text{LayerNorm}(X_t + S_t)$	$X_t = \text{LayerNorm}(X_t + S_t)$
$Y_t = \text{MLP}(X_t)$	$Y_t = \text{MLP}(X_t)$
$Y_t = \text{LayerNorm}(Y_t)$	
Return: $X_t + Y_t$	Return: $S_t + Y_t$

The STATM in STATM-SAVi /SAVi++ employs post-normalization, with the residual structure applies to the last MLP layer of the module. On the other hand, the STATM in STATM-STEVE utilizes pre-normalization, where S_t and M_t share normalization weights, and the entire module applies a residual structure. The size of the key(k), query(q), and value(v) in the spatiotemporal attention for STATM-SAVi is 128, while in STATM-STEVE, it is 192.